Journal of Alloys and Compounds 521 (2012) 55–59

Contents lists available at SciVerse ScienceDirect

Journal of Alloys and Compounds

journal homepage: www.elsevier.com/locate/jallcom

Self-nanoscaling in FeCo alloys prepared via severe plastic deformation

Narayan Poudyal[a,**], Chuanbing Rong[a], Ying Zhang[a,b], Dapeng Wang[a], M.J. Kramer[b], Rainer J. Hebert[c], J. Ping Liu[a,*]

[a] Department of Physics, University of Texas at Arlington, Arlington, TX 76019, USA
[b] Division of Materials Science and Engineering, Ames Laboratory, Iowa State University, Ames, IA 50011, USA
[c] Department of Chemical, Materials and Biomolecular Engineering, University of Connecticut, Storrs, CT 06269, USA

ARTICLE INFO

Article history:
Received 25 October 2011
Received in revised form 3 January 2012
Accepted 4 January 2012
Available online 12 January 2012

Keywords:
FeCo alloys
Nanocrystalline materials
Soft magnetic materials

ABSTRACT

Nanocrystalline $Fe_{100-x}Co_x$ (x = 20, 35, 50, 60) alloys have been prepared by mechanical alloying of Fe and Co powders via high energy ball milling. The alloy formation process and microstructure evolution of the samples have been investigated. Energy filtered transmission microscopy (EFTEM) observations revealed the strip formation of the Fe and Co phases at an initial stage of milling. The final grain size of the equiaxed grains in the obtained alloys reached 8 nm upon milling for 20 h. The saturation magnetization of the mixtures of Fe and Co increases with milling time, indicating an increasing homogeneity in composition and the phase formation. It is found that the saturation magnetization is also dependent on the Co content, which reaches the highest value of 240 emu/g at $Fe_{65}Co_{35}$. The phase transformation of the as-prepared FeCo alloys was also studied using differential scanning calorimetry.

1. Introduction

Nanocrystalline materials exhibit unique magnetic, electric and optical properties due to the ultrafine crystallite grains and the significant fraction of atoms in grain boundaries [1–3]. These properties are extremely sensitive to the materials morphology. FeCo nanocrystalline materials with controlled morphology have potential applications in advanced materials and devices, such as ultrahigh-density magnetic recording media, exchange-coupled nanocomposite magnets, and microwave devices due to the high saturation magnetization, high permeability, and high Curie temperatures [4–9]. Nanostructured FeCo alloy powders have been synthesized through various techniques including chemical synthesis, rapid solidification, inert gas condensation, and ball milling [4–6,10–12]. High-energy ball milling has been proven to be one of the most efficient methods for preparing nanocrystalline materials and alloys [9,13]. It has been reported that for long enough milling time, mechanical alloying can be successfully used for the synthesis of various metal–metal systems [13,14] including FeCo [15–17]. However, the morphology evolution due to the intensive ball milling has not been investigated in detail. In this paper, we report the correlation between morphology and the magnetic properties of nanostructured FeCo alloys prepared by high energy ball milling as a function of milling time.

2. Experimental procedures

The starting elemental powders of particle sizes from ~10 to 45 μm are commercially available Fe with 98% purity and Co with 99.5% purity. The elemental Fe and Co powders were milled in a SPEX 8000 M Mixer/Mill (60 Hz model) sealed under a protective argon atmosphere using 440C hardened steel balls vial. The compositions of the initial powder mixtures were $Fe_{100-x}Co_x$ (x = 20, 35, 50, and 60). The weight ratio of powder to balls was around 1:20. The milling time was varied from 0.5 to 20 h. The ball milling process has two purposes: to make FeCo alloys and to reduce the grain sizes via severe plastic deformation. The morphology and crystalline structure were characterized by transmission electron microscopy (TEM), energy-filtered TEM (EFTEM), and X-ray diffraction (XRD) by Rigaku Ultima IV using Cu Kα radiation. The EFTEM was carried out in a FEI scanning transmission electron microscope operated at 200 keV. The energy filtered imaging was performed using a Gatan Tritium GIF system. The Co and Fe were imaged at their respective l3 edges of 708 and 779 eV. Magnetic properties were measured in a superconducting quantum interference device (SQUID) magnetometer with a maximum applied field of 70 kOe. Differential scanning calorimeter (DSC) measurement were carried out by NETZSCH-DSC-404C at the temperature range of 20–1100 °C at a continuous heating rate of 20 °C per minute under the flow of argon gas.

3. Results and discussion

Fig. 1 shows the XRD patterns of FeCo powder mixtures (a) $Fe_{40}Co_{60}$, (b) $Fe_{50}Co_{50}$, (c) $Fe_{65}Co_{35}$ and (d) $Fe_{80}Co_{20}$ respectively, milled for up to 20 h. The peaks of bcc Fe and hcp Co phases are observed when the milling time is less than 2 h. Upon further milling, the peaks were broadened, reflecting the grain size refinement and the strain increase during the milling process. The Rietveld refinement results show that during the first 5 h of milling, the grain size decreases rapidly from micrometers to the nanometer range. Further grain size reduction proceeds slowly and the

* Corresponding author.
** Corresponding author. Tel.: +1 817 272 5219; fax: +1 817 272 3637.
E-mail addresses: narayan@uta.edu (N. Poudyal), pliu@uta.edu (J. Ping Liu).

0925-8388/$ – see front matter © 2012 Elsevier B.V. All rights reserved.
doi:10.1016/j.jallcom.2012.01.026

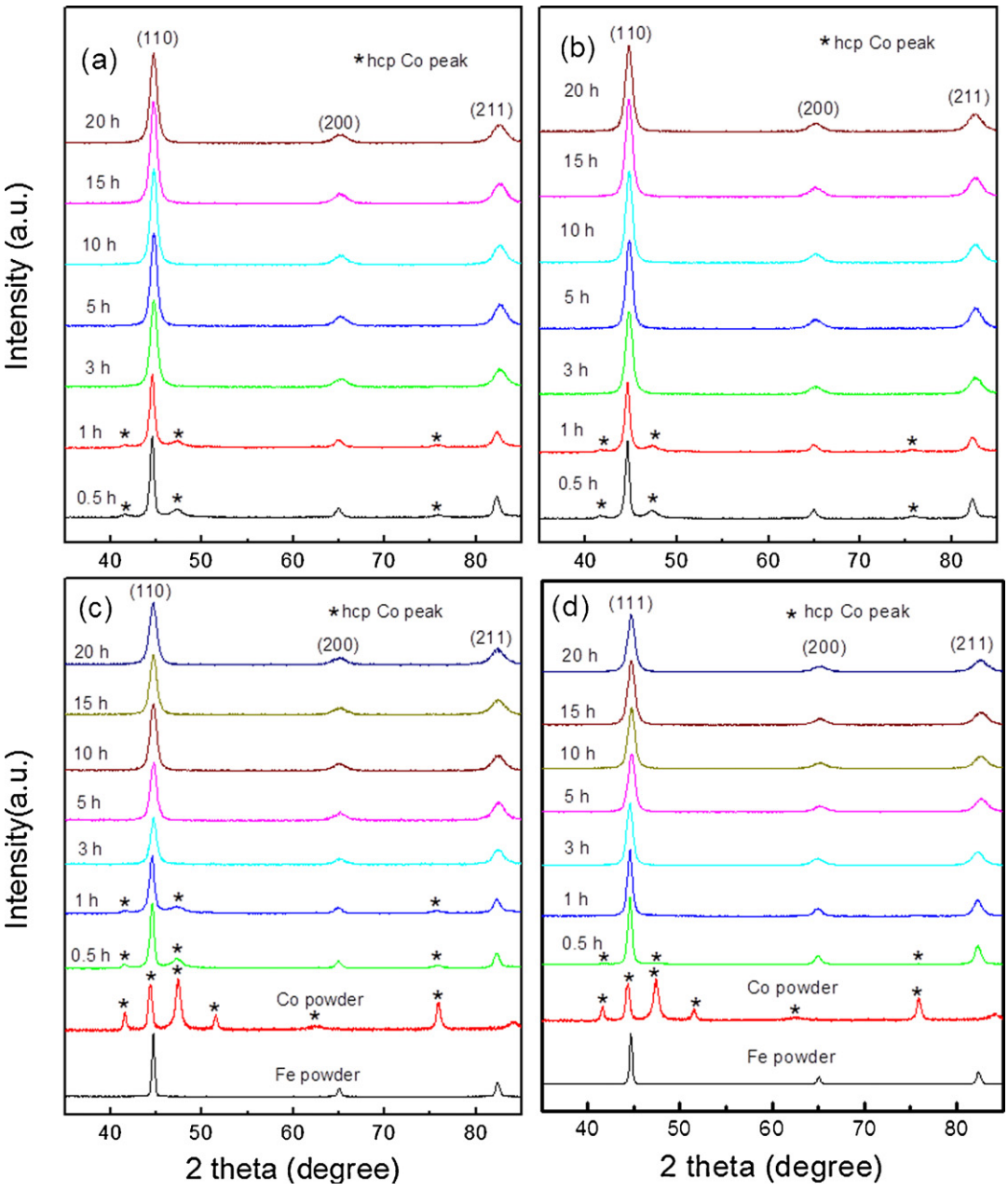

Fig. 1. XRD patterns of FeCo alloys: (a) $Fe_{40}Co_{60}$, (b) $Fe_{50}Co_{50}$, (c) $Fe_{65}Co_{35}$ and (d) $Fe_{80}Co_{20}$ milled for different milling time.

final average grain size is 8 nm when milled up to 20 h as shown in Fig. 2(a). In addition, the complete disappearance of the Co peaks occurs in the powders milled for more than 3 h, suggesting diffusion of Co atoms into the Fe matrix. The decrease in the lattice parameter is consistent with interdiffusion of Co into the Fe forming a bcc FeCo solid [17] (see Fig. 2(b)). The decrease of the lattice parameter is due to the so-called triple-defect disorder [15]. A triple defect consists of one anti-site Co atom with two vacancies on the Co sublattice. Anti-site disorder can be introduced, since no vacant lattice sites are available in the structure suggesting that there is an exchange of Co and Fe atoms during milling leading to a variation of the Co atom neighboring.

The effect of milling time on the microstructure of the $Fe_{65}Co_{35}$ alloy was monitored by the TEM as shown in Fig. 3. Initially, milling of the equiaxed Fe and Co mixture with micron powders leads to the formation of narrow and elongated strips (layered structure) of bcc Fe and hcp Co as seen by bright field TEM images in Fig. 3(a). The selected area diffraction pattern (SADP) inset shows more discrete bcc pattern and weak hcp diffraction spots. The 3 h milled sample shows a smaller separation of the layers than for the initial milling stage as seen in Fig. 3(b) (the light dark contrast is due to diffraction). The SADP inset shows very little hcp Co and the gaps in the ring indicate some grain alignment in this region. With further milling, the nanoscale strips began to break up into isolated equiaxed nanoscale particles. After 20 h, the layers are finer and grains are smaller as seen in Fig. 3(c). The SADP inset shows no indication of an hcp Co phase.

The progressive formation of a layered microstructure and the subsequent break-up of layers into equiaxed particles can be attributed to a system involving two ductile components with different deformation behavior. Benjamin et al. first observed the formation process of alloying in a system involving two different ductile components [19]. In the early stages of milling, the aspect ratio of the ductile powder particles increases and the particles

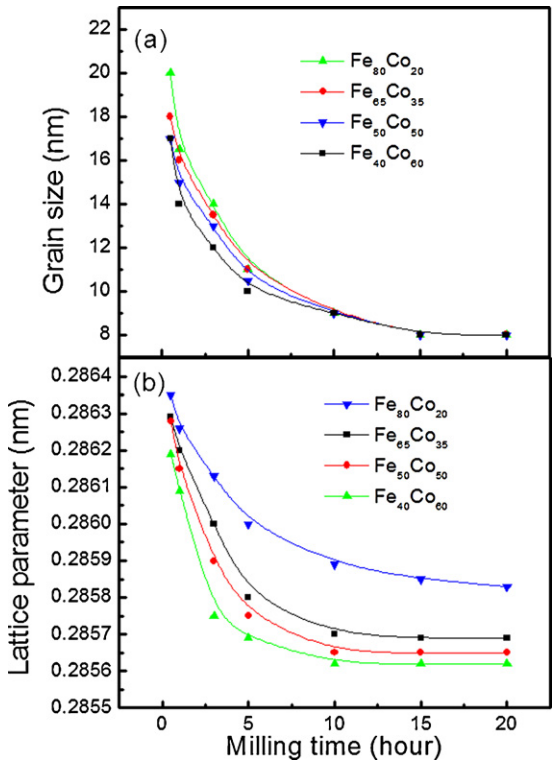

Fig. 2. (a) Grain size and (b) lattice parameter change with milling time for FeCo alloys.

develop into platelets by a micro-forging process. In the next stage, these flattened powder particles cold weld together and form a composite layered structure (strips) of the constituent metals. With increasing milling time, the strips break into particles with more equiaxed shapes. The details of the morphology change from strips into particles are not entirely understood. Several factors could play a role, including the formation and propagation of shear bands during the high strain rate deformation of the layered particles and the formation of multiple necks. The morphology evolution of elemental layers during cold rolling depend on the adjacent layers and their mechanical properties. Very high aspect ratios can be achieved if the flow stresses of adjacent layers are comparable, but the tendency for necking and rupture increase with diverging flow stresses of adjacent layers [20]. The formation of strips during the initial milling, followed by a break-up of the strips could be caused by comparable mechanical properties of the Co and Fe layers during the initial phase and a divergence of the flow stresses after some milling time. This divergence could be associated with the alloying and the strains that develop, but further work is necessary to clarify these factors. The combination of decreased diffusion distances (interlayer spacing), increased lattice defect density, and the heating that occurred during the milling process promote the intermixing kinetics. With further milling, alloying occurs at the atomic level resulting in the formation of the FeCo solid solutions.

Recently, we reported the self-nanoscaling of the soft magnetic phase in SmCo/Fe nanocomposites with brittle/ductile system induced by severe plastic deformation that was similar to the observation presented in this study [9,18]. In particular, energy filtered TEM can be used to produce composition maps with nanometer resolution showing distinct two elements regions. As shown in Fig. 4, the EFTEM analysis revealed a morphology that developed in samples milled for different time. With increasing milling time, Fe and Co powders, which started off as equiaxed micrometer-sized particles, became narrow and elongated and Co atoms mixed into the Fe layers (see Fig. 4(a) and (b) for 1 h milled sample). After 3 h milling, the layering is finer and the grains are more obvious. EFTEM still shows some weak chemical segregation as seen in Fig. 4(c) and (d). For longer milling times, imaging of the microstructure required the higher magnification of the TEM. Samples milled for 20 h showed improved homogeneity (as seen in Fig. 4(e) and (f)) due to the diffusion of Co atoms into the Fe phase leading to the formation of the disordered bcc FeCo solid solution. It should be noted that the composition contrast in Fig. 4(e) and (f)) for Fe and Co maps are almost the same (the dark contrast in Fe map is also dark in Co map and the bright area is bright in the both). This suggests that the contrast might be attributed to the thickness effect of the observed sample. This is consistent with observation of very rough surface in bright field TEM image as seen in Fig. 3(c). The morphology change with milling time of samples with different content of Co by EFTEM is under study which will be reported elsewhere.

The DSC scans of the 20 h milled samples performed up to 1100 °C confirmed the solid solution formation as shown in Fig. 5(a). The broad exothermic peaks occur for all samples that spread over the temperature range 100–550 °C. This behavior originates from recovery, strain relaxation, and grain growth. In the DSC traces of the milled samples, two main peaks were observed. The first peak is broad, endothermic and has a peak maximum of about 717 to 725 °C, which indicates the disordered α-bcc(A1) to ordered α′-CsCl(B2)-type structure transformation for milled samples of $Fe_{100-x}Co_x$ (x = 35–60), except for the $Fe_{80}Co_{20}$ composition, which has a fcc structure (γ-Fe and α-Co) (see Fig. 5(a)). This is in accordance with the Fe–Co phase diagram where the α-Fe–Co solid solution phase transforms from a disordered to an ordered phase for compositions x = 40–60% Co [21]. The second endothermic peak in the continuous heating DSC curve is in the temperature range from 968 to 992 °C (for all milled samples) and is related to the α′-bcc transformation into γ-fcc FeCo and with the change from ferromagnetic to a non-ferromagnetic phase.

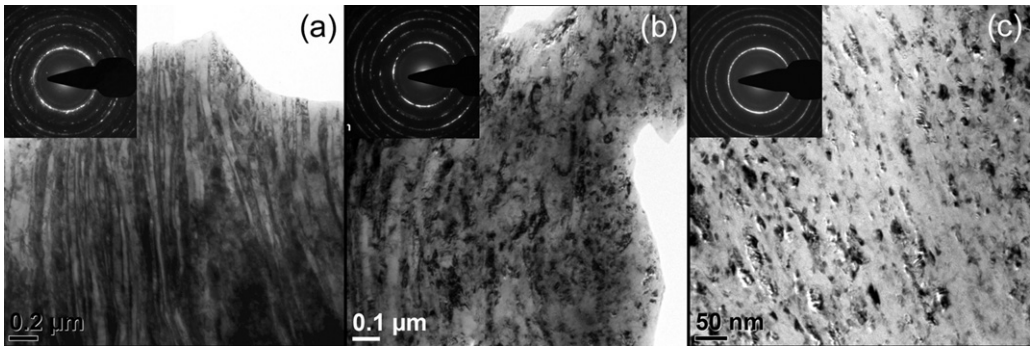

Fig. 3. Bright field TEM images of $Fe_{65}Co_{35}$ alloy milled for (a) 1 h, (b) 3 h and (c) 20 h. Insets show the selected area diffraction patterns.

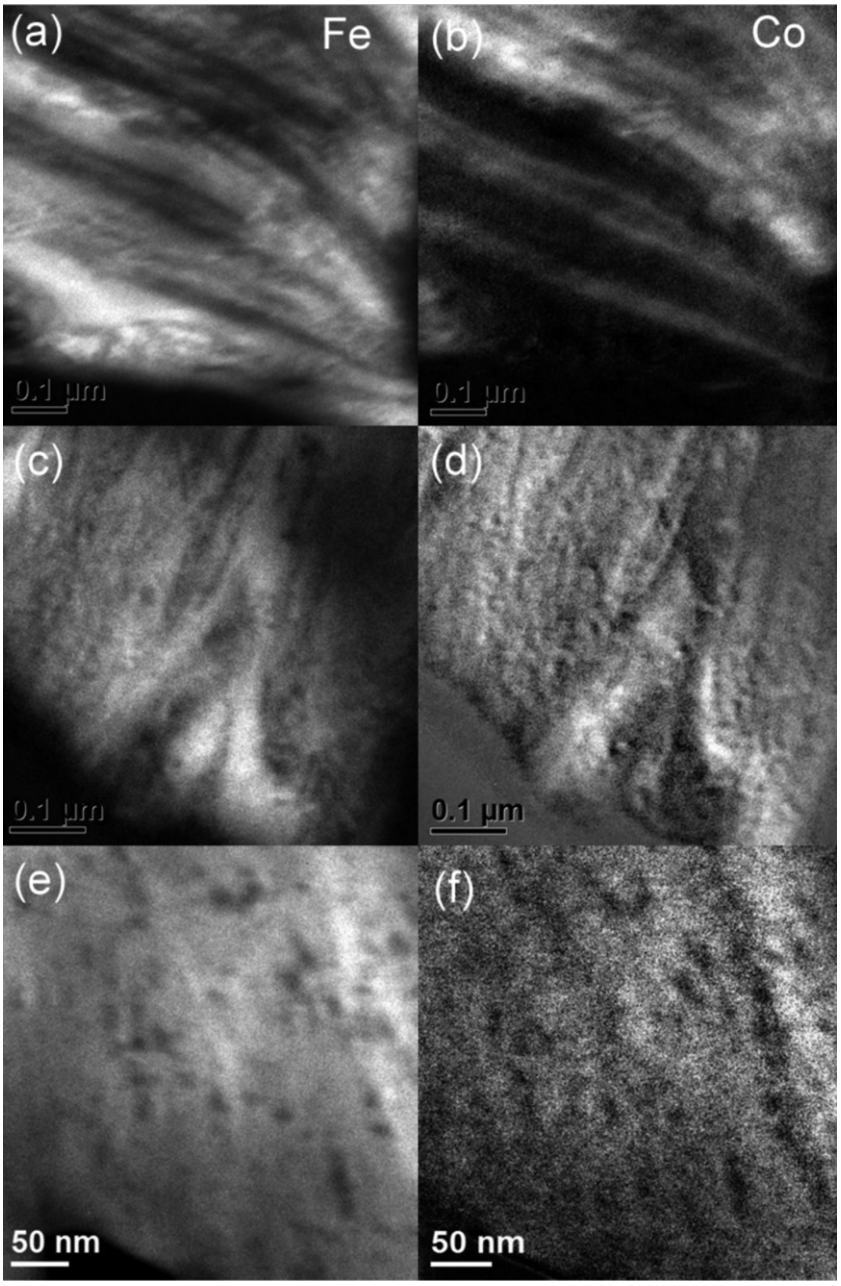

Fig. 4. EFTEM of Fe and Co maps for the same areas showing the distribution of Fe (left column) and Co (right column) with different milling times. The FeCo samples were prepared by milling (a) and (b) for 1 h, (c) and (d) for 3 h and (e) and (f) for 20 h with $Fe_{65}Co_{35}$.

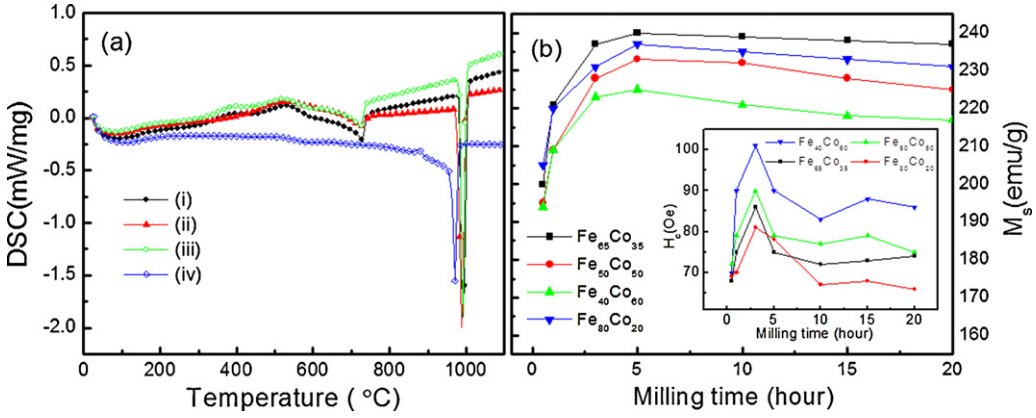

Fig. 5. (a) DSC traces of the as-milled FeCo alloys: (i) $Fe_{40}Co_{60}$, (ii) $Fe_{50}Co_{50}$, (iii) $Fe_{65}Co_{35}$ and (iv) $Fe_{80}Co_{20}$ and (b) saturation magnetization of FeCo alloys with different compositions milled up to 20 h (inset gives the dependence of coercivity on milling time of FeCo alloys).

The progress of alloying process between elemental Fe and Co powders during the milling process was also monitored by measuring the change in saturation magnetization as given in Fig. 5(b). The magnetization increases monotonically with the milling time up to 5 h and then slightly decreases afterwards. The highest saturation magnetization values of $Fe_{100-x}Co_x$ with $x = 20$, 35, 50 and 60 were found to be 232, 240, 236 and 224 emu/g, respectively, for samples milled for 5 h. The increase in the magnetization upon milling should be related to reduction of grain size that facilitates diffusion of Co into Fe leading to improved homogeneity in FeCo as observed from TEM analysis. The decrease in saturation magnetization of FeCo samples milled longer than 5 h might be attributed to an increment of induced structural defects and disordered bcc phase owing to severe plastic deformation of powders. The inset in Fig. 5(b) shows the variation of the coercivety (H_c) of FeCo powder mixtures with different content of Co as a function of milling time. It can be seen that the maximum value of H_c is observed after 3 h of milling and H_c decreases with decreasing grain size for extended milling time. The H_c enhancement for short milling time may be related to the presence of hcp Co phase at the initial stage of milling and to the decrease of grain size of Co as observed by XRD and TEM, since the hcp structure has larger magnetocrystalline anisotropy than the fcc phase. Additionally, H_c increases with increasing Co content for a given milling time. The coercivity value ranges from 80 to 115 Oe for $Fe_{80}Co_{20}$ and $Fe_{40}Co_{60}$, respectively, when they were milled for 3 h.

4. Conclusion

In conclusion, nanocrystalline $Fe_{100-x}Co_x$ ($x = 20$, 35, 50, 60) alloys have been synthesized via mechanical alloying of the Fe and Co powders by high energy ball milling. The microstructure and magnetic properties development of the samples with milling time have been investigated. EFTEM observations showed strip formation of the Fe and Co phases at an initial stage of milling. On further milling Co dissolves into the Fe matrix and forms a disordered FeCo solid solution with equiaxed grains of about 8 nm in size upon 20 h of milling. Both coercivity and saturation magnetization of the as-milled FeCo alloys increase with increasing milling time at initial stage and reach at the maxima at around 3 h and 5 h milling time respectively before slightly decrease upon further milling. The coercivity and saturation magnetization of the as-milled FeCo alloys are also dependent on the Co content. A maximum magnetization value of 240 emu/g for $Fe_{65}Co_{35}$ is obtained.

Acknowledgments

This work has been supported in part by the US Office of Naval Research/MURI project under grant N00014-05-1-0497, DARPA/ARO under grant W911NF-08-1-0249 and ARO under grant W911NF-11-1-0507. This work was also supported by Center of Nanostructured Materials and Characterization Center for Materials and Biology at the University of Texas at Arlington. The microscopy was performed at the Ames Laboratory which is supported in part by the US Department of Energy, Office of Basic Energy Science, under contract DE-AC02-07CH11358.

References

[1] A.I. Boukai, Y. Bunimovich, J. Tahir-Kheli, J.-K. Yu, W.A. Goddard III, J.R. Heath, Nature 451 (2008) 168.
[2] A.I. Hochbaum, R. Chen, R.D. Delgado, W. Liang, E.C. Garnett, M. Najarian, A. Majumdar, P. Yang, Nature 451 (2008) 163.
[3] E.V. Shevchenko, D.V. Talapin, N.A. Kotov, S. O'Brien, C.B. Murray, Nature 439 (2006) 55.
[4] G.S. Chaubey, C. Barcena, N. Poudyal, C.B. Rong, J. Gao, S. Sun, J. Ping Liu, J. Am. Chem. Soc. 129 (2007) 7214.
[5] C. Desvaux, C. Amiens, P. Fejes, P. Renaud, M. Respaud, P. Lecante, E. Snoeck, B. Chaudret, Nat. Mater. 4 (2005) 750.
[6] N. Poudyal, C.B. Rong, J. Ping Liu, J. Appl. Phys. 109 (2011) 07B526.
[7] S. Sun, C.B. Murray, D. Weller, L. Folks, A. Moser, Science 287 (2000) 1989.
[8] H. Zeng, J. Li, J. Ping Liu, Z.L. Wang, S. Sun, Nature 420 (2002) 395.
[9] C.B. Rong, Y. Zhang, N. Poudyal, X. Xiong, M.J. Kramer, J. Ping Liu, Appl. Phys. Lett. 96 (2010) 102513.
[10] M. Han, H. Lu, L. Deng, Appl. Phys. Lett. 97 (2010) 192507.
[11] Y. Jing, H. Sohn, T. Kline, R.H. Victora, J.P. Wang, J. Appl. Phys. 105 (2009) 07B305.
[12] Y.D. Kim, J.Y. Chung, J. Kim, H. Jeon, Mater. Sci. Eng. A291 (2000) 17.
[13] C. Suryanarayana, Progr. Mater. Sci. 46 (2001) 1.
[14] C. Kuhrt, L. Schultz, J. Appl. Phys. 73 (1992) 1975.
[15] S. Azzaza, S. Alleg, H. Moumeni, A.R. Nemamcha, J.L. Rehspringer, J.M. Greneche, J. Phys.: Condens. Matter 18 (2006) 7257.
[16] A. Zeleňáková, D. Olekšáková, J. Degmová, J. Kováč, P. Kollár, M. Kusý, P. Sováka, J. Magn. Magn. Mater. 316 (2007) e519.
[17] H. Moumeni, S. Alleg, J.M. Grenèche, J. Alloys Compd. 386 (2005) 12.
[18] C.B. Rong, Y. Zhang, N. Poudyal, I. Szlufarska, R.J. Hebert, M.J. Kramer, J. Ping Liu, J. Mater. Sci. 46 (2011) 6065.
[19] J.S. Benjamin, T.E. Volin, Metall. Trans. 5 (1974) 1929.
[20] G. Marathe, PhD Thesis, University of Connecticut, 2011.
[21] I. Ohnuma, H. Enoki, O. Ikeda, R. Kainuma, H. Ohtani, B. Sundman, K. Ishida, Acta Mater. 50 (2002) 379.